Chapter 5

Application of AuNP decorated exfoliated WS_2 incorporated PEDOT-PSS electrodes for sensing of Glucose and Aflatoxin B_1

This chapter focuses on highly sensitive, selective, user-friendly and versatile electrochemical sensors for glucose and AF-B_1 based on gold nanoparticle (AuNP) decorated tungsten disulfide (WS_2) incorporated Poly (3,4-ethylenedioxythiophene): polystyrene sulphonic acid (PEDOT-PSS) nanocomposite. Electrochemical Impedance Spectroscopy (EIS) and Cyclic Voltammetry (CV) were used to examine the charge transfer kinetics and electroactive properties of the modified electrodes. The interaction between glucose oxidase (*Glox*) enzyme and D- glucose was monitored via Chronoamperometry. Both capacitive and amperometric sensing techniques were employed to evaluate sensing parameters for AF-B_1 detection. The feasibility of the synthesized biosensors has been tested by evaluating their performance with real samples.

5.1. Introduction

Recently, transition metal dichalcogenides (TMDCs) such as, WS_2, WSe_2, MoS_2, $MoSe_2$ have gained significant interest in the field of electrochemical sensing because of their large specific surface areas, fast electron transfer kinetics, and high electrical conductivity [1]. In contrast to their molybdenum counterparts (MoS_2 and $MoSe_2$), tungsten dichalcogenides (WS_2 and WSe_2) demonstrate superior electron transfer properties [2]. Offering diverse scope of applications, the 2D WS_2 material of monolayer form is essentially a trilayer structure in which W atoms are surrounded by S atoms forming a sandwich- like (S-W-S) arrangement. Electrochemical activity of WS_2 is predominantly located in the edge surface due to the presence of chemically active dangling bonds. These dangling bonds can interact more readily with other molecules or substrates, making the edges of TMDCs particularly reactive in various electrochemical processes. The high density of edge sites in TMDCs makes them attractive for applications such as catalysis, sensing, and energy storage. Again, it was suggested that the presence of surface defects in the WS_2 have a higher tendency to introduce electrochemical active sites [3]. As compared to graphene, TMDCs have a large and adjustable bandgap, which makes it possible to reduce leakage current compared to graphene and ensure a higher level of sensitivity and accuracy [4] Similar to graphene, TMDCs have layered structures, but a monolayer of a TMDC comprises three independent layers of atoms. While TMDCs are held together by relatively weak van der Waals forces, they have the advantage of facilitating easy exfoliation into single layers or flakes of a few layers, unlike graphene

oxide. As a result, this provides a large surface area offering numerous potential binding sites to the electrodes, thus enabling excellent sensitivity of electrochemical sensors for detecting various biomolecules. Moreover, layered WS_2 possess higher conductivity yielding excellent electron transfer kinetics while GO is less conducting due to the presence of various oxygen containing functional groups. Unlike graphene, WS_2 demonstrates lower toxicity and is biodegradable and rapidly excreted [5,6]. Further, Teo et al. found that the cytotoxicity of TMDCs (such as MoS_2, WS_2, and WSe_2) is lower than that of graphene analogs [7]. Moreover, the electrochemical activity of tungsten dichalcogenides (WS_2, WSe_2) is superior in many ways to their molybdenum counterparts (MoS_2, $MoSe_2$) [8]. Introduction of WS_2 into PEDOT-PSS enabled charge carriers to move efficiently along the polymer chains. This significantly enhances charge transfer within the composite system increasing overall conductivity of the 2D-polymer matrix [9,10]. The WS_2 nanosheets provide high surface to volume ratio, easy monolayer separation due to weak binding forces (van der Waals) [11] and higher conductivity. Moreover, higher surface area leads to increased electroactive sites, which improves the overall electrochemical response. Polymers doped with WS_2 often exhibit enhanced stability and durability making the system robust and efficient for a variety of electrochemical based applications. Gold nanoparticle (AuNP) is said to have excellent charge transfer property, catalytic abilities, as well as a high degree of biocompatibility [12-14] and adds surface area in the composites. Since AuNPs possess high conductivity, catalyzing activity, chemical stability and biocompatibility, the cooperative effects of Au and the enzyme biosensor can result in enhanced sensing performance [15,16].

The present work deals with the fabrication and development of a robust, portable, and reliable biosensor probes based on AuNPs decorated WS_2 modified PEDOT-PSS based electrode. Therefore, the primary aim of this study is to improve the sensing characteristics of amperometric glucose sensors highlighting sensitivity, selectivity and LOD evaluated through chronoamperometry. For AF-B_1 detection, both amperometric and capacitive measurements have been highlighted and evaluated for augmented sensitivity.

(A) Glucose sensor

5.2. Electrochemical studies of the Glucose biosensors

To understand the electroactive properties, CV was carried out for both the prepared WS_2/PEDOT-PSS and AuNP/WS_2/PEDOT-PSS electrode at a scan rate of 20 mV/s under potential window from -0.2 V to 1.2 V in 0.1 M PBS (pH=7.4) as electrolyte. Again, to study the change transfer kinetics at the electrode and electrolyte interface, multifrequency impedance spectroscopy was performed with an ac signal of 10 mV within frequency range from 1 Hz to 1 MHz in PBS electrolyte. The interaction between glucose and glucose oxidase was monitored by measuring the amperometric response through chronoamperometry.

5.2.1. Cyclic voltammetry (CV) analysis of Glucose sensor

The CV plots of WS_2/PEDOT-PSS/ITO and AuNP/WS_2/PEDOT-PSS/ITO electrodes after each step of processing is displayed in Figure 5.1. CV curves of WS_2/PEDOT-PSS electrode after each process steps of sensor fabrication such as: after glutaraldehyde treatment, after enzyme (glucose oxidase) immobilization and after enzyme-glucose interaction can be found in Figure 5.1 (a).

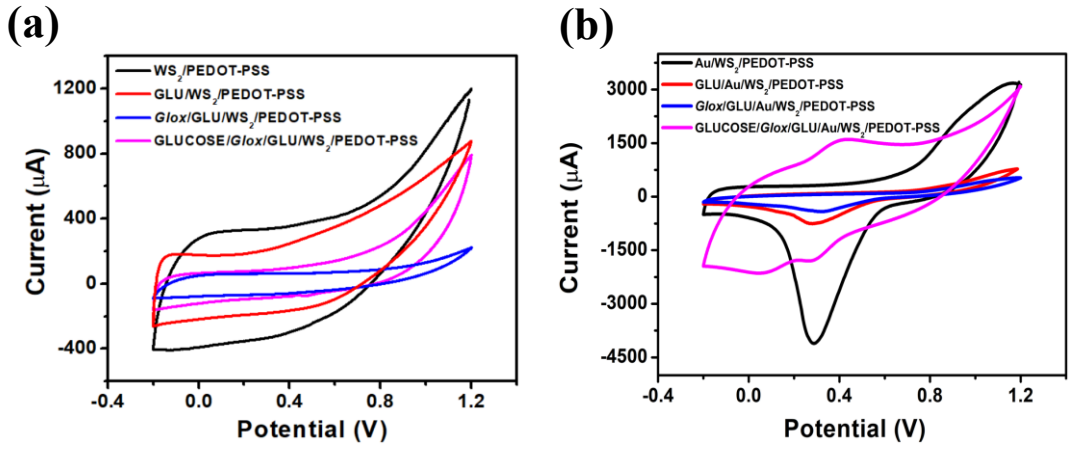

Figure 5.1: Cyclic voltammetry plots of (a) *GlOx*/GLU/WS_2/PEDOT-PSS/ITO sensor after each process step, with final step of 32 µM glucose interaction, (b) *GlOx*/GLU/AuNP/WS_2/PEDOT-PSS/ITO sensor after each process step and with addition of 440.67 µM glucose.

Adsorption of the thin layer of glutaraldehyde depicted in a decrease in the area under the CV curve due to poor charge transfer at the interface. Similarly, enzyme immobilization treatment leads to lesser charge transfer at the interface owing to its large molecular size which resulted in drastic decrement in the area under the CV curve. However, there was an increment in the area after glucose oxidase enzyme and glucose interaction suggesting increased charge transfer between glucose and the immobilized enzyme.

CV curves for the AuNP/WS_2/PEDOT-PSS electrode after every process step of sensor fabrication is displayed in Figure 5.1 (b). The intensity of the reduction peak decreases after glutaraldehyde treatment and glucose oxidase immobilization step respectively as in the case of AuNP/GO/PEDOT-PSS/ITO electrode in chapter 4. However, interaction of glucose oxidase enzyme with analyte glucose changed the CV plot with one new oxidation peak at around 0.45 V and one more reduction peak at around 0V with increase in the area under the CV curve. These peak currents were observed to increase with glucose concentration whereas the Au reduction peak current remained the same. *GlOx* converts glucose into D-glucono-1,5-lactone and H_2O_2, resulting in change in electron concentration, change in the oxidation peak can be observed [17-20].

FAD encounters a redox reaction with biomolecules, involving coupling of two protons and two electrons as shown in equation 4.1, Chapter 4. This suggests that the electrochemical response is attributed to oxidation of H_2O_2, which is released as a result of enzymatic reaction of glucose oxidase with glucose.

Upon the addition of glucose, the enzyme-catalyzed reaction between FAD and glucose results in an increase in redox peak current, as explained by the following equations

$$\text{Glucose} + \textit{GlOx}\ (\text{FAD}) \rightarrow \text{Gluconolactone} + \textit{GlOx}\ (\text{FADH}_2) \quad (5.1)$$

$$\text{GlOx}\ (\text{FADH}_2) + \text{O}_2 \rightarrow \text{GlOx}\ (\text{FAD}) + \text{H}_2\text{O}_2 \quad (5.1.1)$$

$$\text{i.e., } \beta\text{-D-glucose} + \text{O}_2 \rightarrow \text{D-glucono-1,5-lactone} + \text{H}_2\text{O}_2 \quad (5.1.2)$$

5.2.2. Impedance studies of the sensor electrodes

The impedance spectra of WS_2/PEDOT-PSS and AuNP/WS_2/PEDOT-PSS over ITO electrode after every process step of sensor fabrication such as: after glutaraldehyde treatment, after enzyme immobilization and after enzyme – glucose interaction is

displayed in Figure 5.2 (a) and (b) respectively. Here, the equivalent circuit parameters are: R_1 is the series resistance including contact resistance while R_{ct} is the charge transfer resistance. Both Q_2 and Q_3 are constant phase elements. Q_2 is due to the formation of a double layer capacitor at the interface, Q_3 is the space charge layer modification between PEDOT and PSS rich grains in presence of WS_2 and Au. Here, W_3 represents the Warburg impedance originating due to diffusion inside the layered interconnected polymer structure. Unlike GO which has all the atoms in the same plane, each monolayer of WS_2 consists of one plane of tungsten atoms sandwiched between two planes of sulphur atoms with a covalent bonding arranged in a trigonal prismatic network. The monolayers are bonded to each other by weak van der Waals forces that can easily be broken facilitating diffusion of ions. In the impedance spectra the diameter of the semicircle represents the charge transfer resistance (R_{ct}) while the diffusive part is represented by Warburg impedance at lower frequency region. R_{ct} for WS_2 composite electrode is lesser compared to GO composite electrode. The R_{ct} value of WS_2/PEDOT-PSS electrode is 22.45 Ω while it decreases to 13.43 Ω after electrodeposition of AuNPs over the surface of the WS_2/PEDOT-PSS electrode as a result of better charge transfer at the interface after incorporation of gold, mentioned in chapter 3. The impedance spectra of Au/WS_2/PEDOT-PSS/ITO electrode after every process step of sensor fabrication is displayed in Figure 5.2 (b) with equivalent circuit parameters shown in Table 5.1.

Table 5.1: Fitted parameters from EIS spectra for AuNPs deposited WS_2/PEDOT-PSS/ITO electrode after every process step of sensor fabrication.

Serial number	Electrode	R_1 (Ω)	R_{ct} (Ω)	Q_2 ($\times 10^{-6}$) S.s^n	Q_3 ($\times 10^{-3}$) S.s^n	W_3 (x10^{-6}) (S.s$^{1/2}$)
1	GLU/AuNP/WS_2/PEDOT-PSS	29.01	52.69	9.991, n = 0.996 $Q_2{}^n$ = 9.89	4.639, n = 0.5 $Q_3{}^n$ = 2.1	914.8
2	*GlOx*/GLU/AuNP/ WS_2/PEDOT-PSS	48.84	241.2	27.41, n = 0.858 $Q_2{}^n$ = 17.12	0.281, n = 0.953 $Q_3{}^n$ = 0.29	2067
3	GLUCOSE/*GlOx*/GLU/ AuNP/WS_2/PEDOT-PSS	28.69	135	14.46, N = 0.952 $Q_2{}^n$ = 12.71	0.676, n= 0.690 $Q_3{}^n$ = 0.76	1041

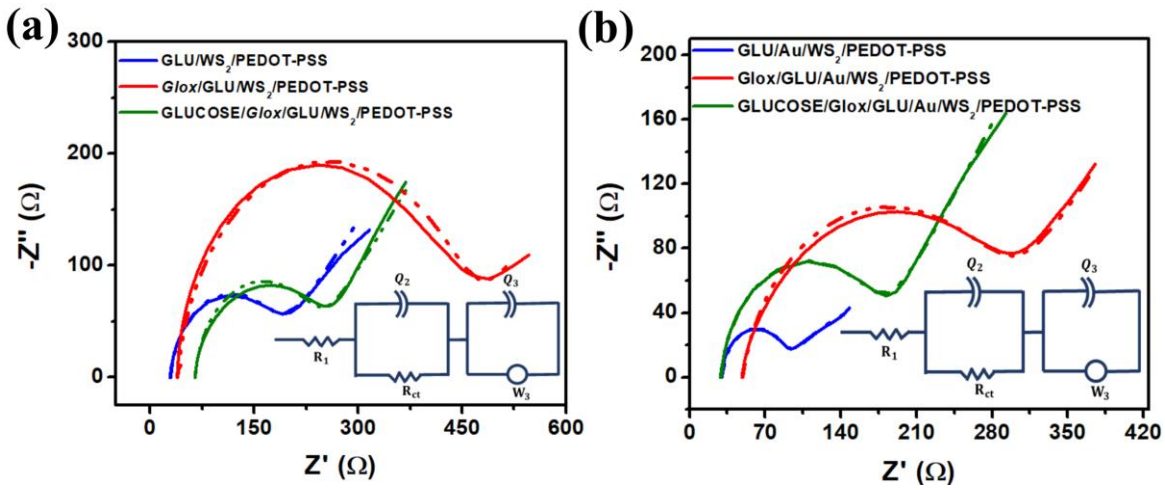

Figure 5.2: Impedance response of (a) WS_2/PEDOT-PSS/ITO sensor (with addition of glucose concentration 32 µM), (b) AuNP/WS_2/PEDOT-PSS/ITO sensor (with addition of glucose concentration 440.67 µM) after each process steps.

The R_{ct} value increases from 13.43 Ω to 52.69 Ω after glutaraldehyde treatment for the AuNP/ WS_2/PEDOT-PSS electrode while after *GlOx* enzyme immobilization the R_{ct} value enhanced up to 241.2 Ω due to adsorption of enzyme over the surface of the GLU/AuNP/WS_2/PEDOT-PSS. After enzyme and glucose interaction the R_{ct} value reduced to 135 Ω as glucose oxidase oxidizes glucose resulting in better charge transport at the interface. The constant phase element Q_3 value decreases after glutaraldehyde treatment and enzyme immobilization due to changes in the space charge layer at the interface of electrode and electrolyte. The Q_2 value steadily increases after glutaraldehyde and enzyme layer deposition. However, reaction between enzyme and glucose leads to slight decrease in Q_2 value as a result of increased charge transfer. The W_3 value increases after glutaraldehyde treatment followed by enzyme immobilization as a result of increase in the diffusional impedance, but it decreases after enzyme – analyte interaction.

5.3. Glucose oxidizing activity of the fabricated sensor electrode

CV plots were recorded with the glucose oxidase immobilized AuNP/WS_2/PEDOT-PSS/ITO electrode at different glucose concentration, shown in Figure 5.3. CV was recorded with various concentration of glucose such as: 100 µM, 300 µM, 500 µM, 700 µM, 900 µM and 1 mM in PBS electrolyte. The curve shows increasing oxidation peak at around 0.45 V and reduction peak at 0 V with increased glucose concentration.

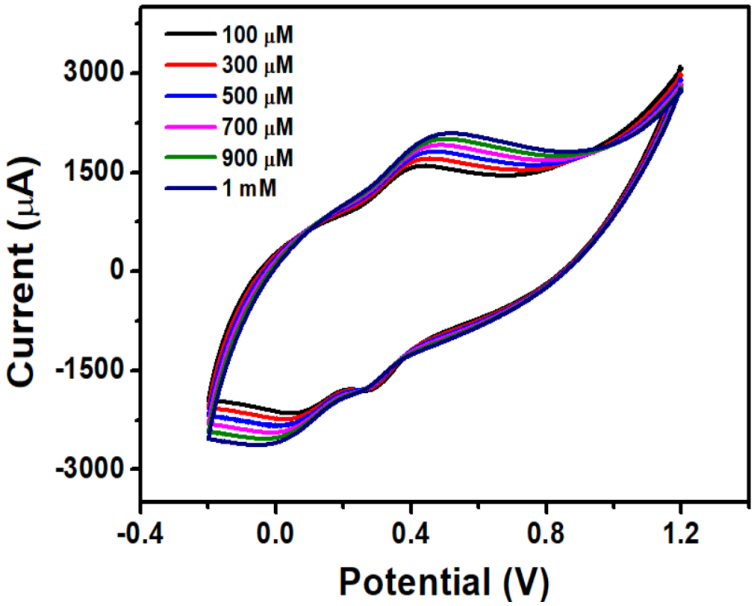

Figure 5.3: Cyclic voltammetry plot of *Glox*/GLU/AuNP/WS_2/PEDOT-PSS bioelectrode at different glucose concentrations.

Increase in the oxidation peak current is clearly observed with respect to different concentration of glucose within the potential range from 0.4 V to 0.5 V. From the fact that the reduction peak due to Au nanoparticles remained same with various additions of glucose concentration, it can be presumed that electron transfer effects on WS_2 are more in the composite electrode.

5.4. Amperometric detection of glucose

For fast and direct measurement of glucose concentration, the amperometric studies of the prepared electrodes towards glucose detection was carried out via chronoamperometry. The chronoamperometry behaviour for the WS_2/PEDOT-PSS/ITO electrode, performed at a potential of 0.6 V is shown in (Figure 5.4). As can be found, the WS_2/PEDOT-PSS/ITO electrode offers poor linearity as seen from the current response to each addition of glucose. The amperometry plot for the *Glox*/GLU/AuNP/WS_2/PEDOT-PSS electrode is displayed in Figure 5.5 (a). Different concentrations of glucose were injected as a function of time can be found in Figure 5.5 (a). Chronoamperometry was performed at a working potential of 0.45 V vs. Ag/AgCl for the glucose oxidase (3 mg mL^{-1}) immobilized GLU/AuNP/WS_2/PEDOT-PSS electrode. The baseline shows an increase in the current response at each step with each subsequent addition of glucose. Further, the selectivity of the sensor was examined by adding ascorbic acid at position A. When ascorbic acid (20

µL) was added the sensor did not show any significant change in the current response yielding its selectivity towards glucose only.

The change in the current response with respect to the concentration of glucose for the *Glox*/GLU/AuNP/WS_2/PEDOT-PSS sensor is shown in Figure 5.5 (b). As can be mentioned, WS_2/PEDOT-PSS electrodes showed poor selectivity and linearity. After incorporation of AuNP over the surface of the WS_2/PEDOT-PSS electrode, the linearity and selectivity were found to be better. The linear fit (R^2: 0.9989) was done for the change in the current response vs the concentration with 3% error bar (Figure 5.5 (b)). The LOD of the sensor was calculated by using the formula LOD = $3.3\times\sigma/S$, where σ = standard deviation, and m = slope of the regression line [21]. The LOD was found to be 1 µM with a higher sensitivity of 13.1 µA μM^{-1}. The sensor showed a wide linear range within 0.74 to 440.67 µM towards oxidation of glucose.

For comparison with clinical estimates of glucose, linear regression plot (R^2: 0.9989) of Conc. (both µM and mg/dL) vs ΔI for AuNP/WS_2/PEDOT-PSS/ITO sensors is displayed in Figure 5.5 (c). AuNP/WS_2/PEDOT-PSS/ITO sensor depicted a linear range within 0.013 mg/dL - 7.932 mg/dL.

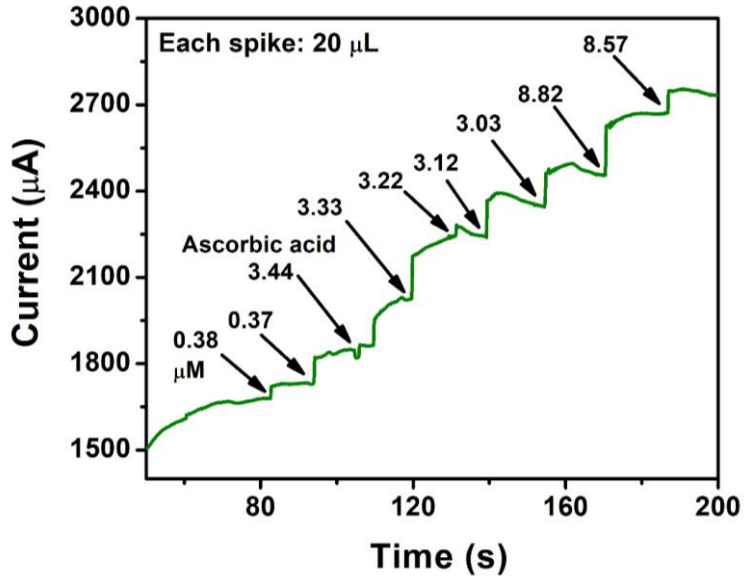

Figure 5.4: Chronoamperommetry plot of WS_2/PEDOT-PSS/ITO electrode at different glucose concentrations in PBS electrolyte.

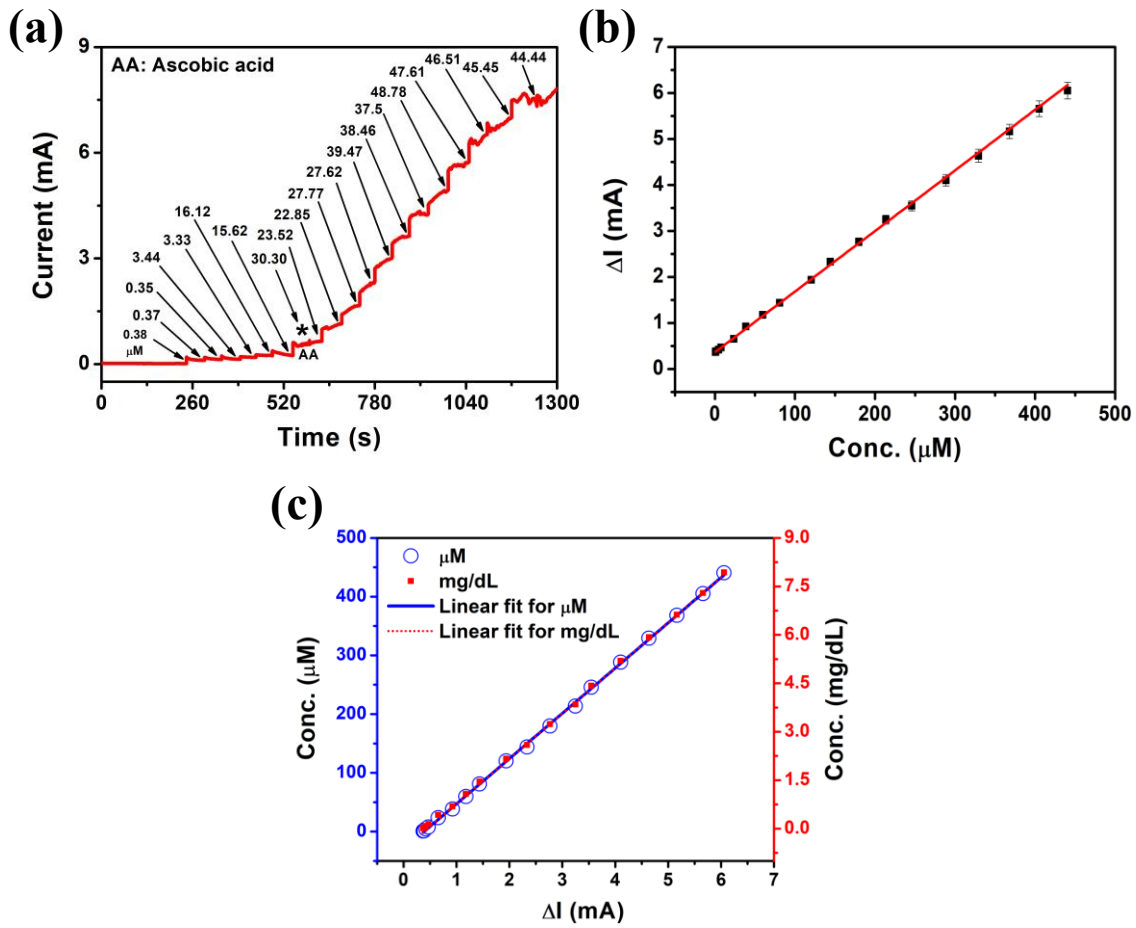

Figure 5.5: (a) Chronoamperometry plots of AuNP/WS_2/PEDOT-PSS/ITO electrode at different concentrations of glucose. (b) Linear regression plot of current vs. concentration for AuNP/WS_2/PEDOT-PSS/ITO biosensor with error bar. (c) Linear regression plot of Conc. (both μM and mg/dL) vs ΔI for AuNP/WS_2/PEDOT-PSS/ITO.

Our study showed that LOD for Au decorated WS_2/PEDOT-PSS/ITO is better than the majority of the reported enzymatic glucose sensors including our previous study, chapter 4. In case of 2D WS_2, easy exfoliation from bulk to a few layers could be facilitating the interlayer separation overcoming the weak Van der Waals forces, resulting in increased surface area in the AuNP/WS_2/PEDOT-PSS/ITO electrode leading to wider sensing range and higher sensitivity compared to GO based composites, AuNP/GO/PEDOT-PSS.

5.5. Selectivity and repeatability

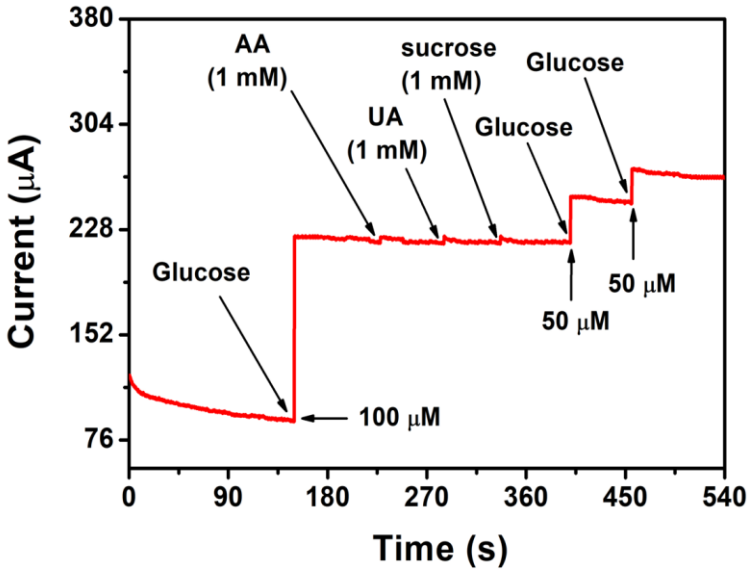

Figure 5.6: Selectivity test in presence of different interference like ascorbic acid (AA), uric acid (UA), sucrose (1 mM of each).

The selectivity test was again carried out by performing chronoamperometry at a potential of 0.45 V on *Glox*/GLU/AuNP/WS_2/PEDOT-PSS sensor in presence of various interference species, including ascorbic acid, sucrose and uric acid (1 mM each), displayed in Figure 5.6. There was no observable shift in the baseline upon the addition of the three different interfering compounds, highlighting the excellent selectivity of the proposed sensor. With an aim to develop a reliable amperometric glucose sensor, repeatability studies were performed with three different AuNP/WS_2/PEDOT-PSS/ITO electrodes and the results are shown in Table 5.2.

Table 5.2: Results of AuNP/WS_2/PEDOT-PSS glucose sensor from repeatable experiment.

Serial number	Electrode	LOD (μM)	Sensitivity (μA μM^{-1})	Linear range (μM)
1	AuNP/WS_2/PEDOT-PSS, sensor 1	1	13.10	0.74-440.67
2	AuNP/WS_2/PEDOT-PSS, sensor 2	1.1	12.97	0.74-440.67
3	AuNP/WS_2/PEDOT-PSS, sensor 3	7.24	18.23	0.74-378.53

5.6. Real sample analysis

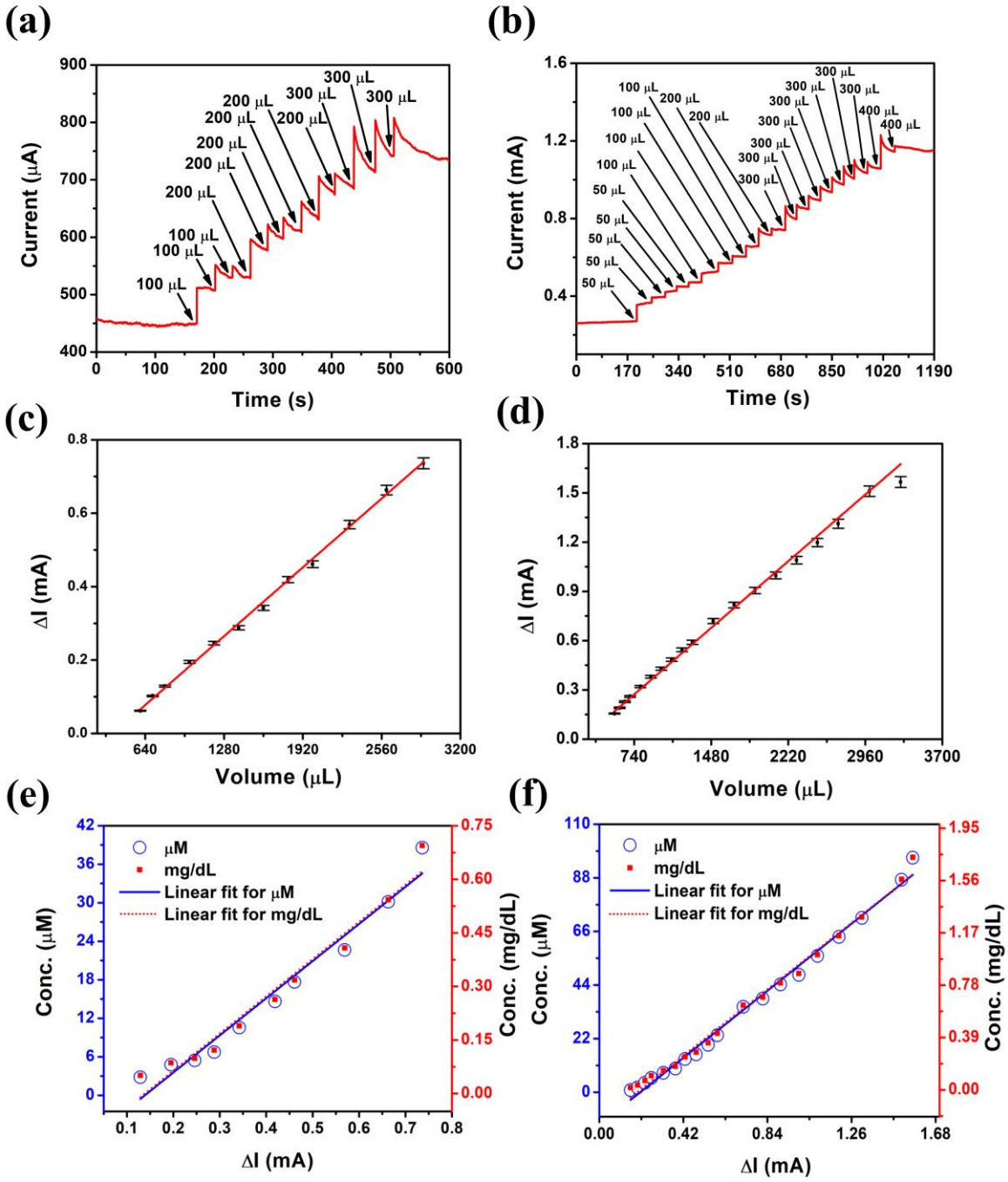

Figure 5.7: Chronoamperometry plots of AuNP/WS_2/PEDOT-PSS/ITO electrode at different volume of salivary sample (a) sample 1, (b) sample 2. Linear regression plot of current vs. volume for AuNP/WS_2/PEDOT-PSS/ITO electrode of (c) sample 1, (d) sample 2 with error bars. Linear regression plot of Conc. (both μM and mg/dL) vs ΔI (e) sample 1 and (f) sample 2.

The developed *Glox*/GLU/AuNP/WS_2/PEDOT-PSS/ITO biosensor was applied to detect glucose in real biological sample without any pre-treatment step. To show the biomedical prospect of the proposed biosensor, human saliva sample was evaluated to detect glucose content. For this study, as mentioned in chapter 4, two participants on volunteer basis were selected; sample 1 is non-diabetic, while sample 2 is diabetic. The saliva sample was obtained from the two volunteers in the morning hours before having food. Each saliva swab was separately mixed with 0.1 M PBS, the remaining solution was shaken well [22]. To remove any contaminant from the saliva solution, the mixture was filtered separately and the filtrate was used for further experiment. Chronoamperometry technique was employed to perform glucose sensing in real samples with Glox/GLU/AuNP/WS_2/PEDOT-PSS/ITO electrodes at a potential of 0.45 V, adding different volumes of samples at intervals. During chronoamperometry, after establishing a stable baseline, varying volumes of saliva solution were injected at different time intervals. The chronoamperometry plot of AuNP/WS_2/PEDOT-PSS/ITO electrode for sample 1 and sample 2 is shown in Figure 5.7 (a) and (b) and corresponding linear regression is displayed in Figure 5.7 (c) and (d) respectively. The linear regression plots (R^2: 0.9958 & 0.9956) of Conc. (both μM and mg/dL) vs ΔI for sample 1 and sample 2 are shown in Figure 5.7 (e, f) respectively. Sample 1 offers a maximum of 38.59 μM (0.695 mg/dL) as regards presence of glucose in saliva, while sample 2 yielded 96.27 μM (1.733 mg/dL). Here also repeatability has been done to validate the results and shown with error bar in the linear plots (Figure 5.7 (b, c)).

(B) Aflatoxin B_1 sensor

5.7. Electrochemical studies of the AF-B_1 immunosensors

CV curves were recorded for the fabricated electrodes at each processing step of sensor fabrication, using 0.1 M PBS as the electrolyte. The measurements were taken at a scan rate of 20 mV/s within a potential range of -0.2 V to 1.2 V [23,24]. Additionally, electrochemical impedance spectroscopy (EIS) was conducted over a frequency range of 1 Hz to 1 MHz, using a 10 mV peak-to-peak AC voltage and a 0 V DC bias. Detection of AF-B_1 antigen was performed utilizing two techniques: transient capacitance measurements at 77 Hz and 1 kHz and differential pulse voltammetry (DPV).

5.7.1. Cyclic voltammetry studies of fabricated Aflatoxin B_1 sensor

The electrochemical behavior of WS_2/PEDOT-PSS/ITO and AuNP/WS_2/PEDOT-PSS/ITO electrodes were analyzed after each processing step, including glutaraldehyde attachment, antibody immobilization, and antigen interaction, using CV within a potential window of -0.2 V to 1.2 V at a scan rate of 20 mV/s. The CV spectra for WS_2/PEDOT-PSS/ITO electrode is shown in Figure 5.8 (a). As can be seen, after adsorption of glutaraldehyde layer over the surface of the WS_2/PEDOT-PSS/ITO, the area under the CV curve declined because of lowered charge transfer events at the interface.

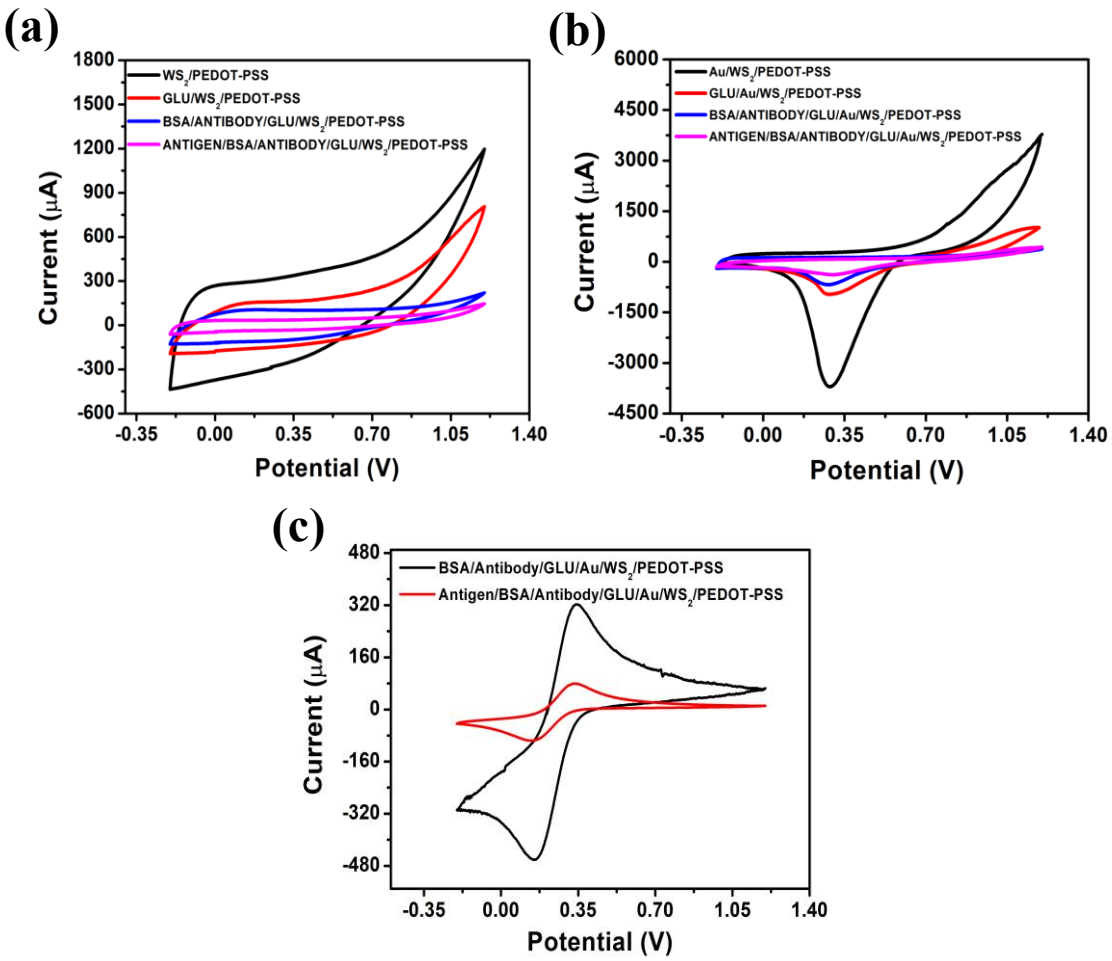

Figure 5.8: Cyclic voltammetry plot of (a) anti-AF-B_1/WS_2/PEDOT-PSS/ITO within a potential window of -0.2 V to 1.2 V and at a scan rate of 20 mV/s. CV plots of anti-AF-B_1/AuNP/WS_2/PEDOT-PSS/ITO sensor in (b) PBS (electrolyte1) after each process step, with final step of injecting antigen concentration. (c) 100 mM PBS and 5 mM $[Fe(CN)_6]^{3-/4-}$ (electrolyte 2) after AF-B_1 addition.

Furthermore, the CV response decreases after antibody treatment and antibody-analyte interaction respectively due to the formation of dielectric layer at the interface which resists the flow of electrons at the electrolyte- electrode interface. The CV was performed for AuNP/WS_2/PEDOT-PSS with electrolyte 1 (PBS) and 2 (PBS+$[Fe(CN)_6]^{3-/4-}$) are displayed in Figure 5.8 (b and c); respectively. The modified electrodes, as shown in Figure 5.8 (c), exhibited well-defined redox peaks, attributed to the electron transfer between the electrode and $[Fe(CN)_6]^{3-/4-}$ solution [Fe(III) ↔ Fe(II) + e^-] [25]. Furthermore, the area under the CV curves decreases following the interaction between anti-AF-B_1 and AF-B_1, attributed to the slower charge transfer at the electrode-electrolyte interface caused by the formation of the immunocomplex. Even without the presence of a redox couple, a systematic decrease in the reduction peak current is observed (Figure 5.8 (b)). The reduction peak observed at 0.289 V decreases after glutaraldehyde adsorption and anti-AF-B_1 immobilization. Following the interaction between the analyte AF-B_1 and anti-AF-B_1, the area under the curve significantly declines, along with the reduction in peak current, indicating a reduced charge transfer at the electrode-electrolyte interface.

5.7.2. Electrochemical Impedance Studies of Aflatoxin B_1 sensor

To explore the electron transfer kinetics at the electrolyte-electrode interface, impedance spectroscopy was carried out for all the prepared electrodes, which is one of the most effective methods to study different features of the synthesized electrodes after surface modifications. The impedance spectra of WS_2/PEDOT-PSS/ITO and Au anchored WS_2/PEDOT-PSS/ITO electrodes after every processing step of sensor fabrication namely, glutaraldehyde treatment, antibody incubation and antibody - analyte immunocomplex formation can be found in Figure 5.9 (a) and (b); respectively. The Nyquist plot contains a semicircular portion with a diffusion spectrum at the higher and lower frequency respectively where the dotted lines are the fitted data. The impedance data are fitted using the inset equivalent circuit where the parameters are: R_1 is series resistance, R_{ct} is the charge transfer resistance, Q_2 and Q_3 are both constant phase element, Q_2 is due to the formation of double layer capacitor at the interface and Q_3 is due to the space charge layer modification within PEDOT and PSS rich grains, W_3 represents Warburg impedance. The equivalent parameters after every process step of the ternary electrode in presence of AuNPs are depicted in Table 5.3.

The charge transfer resistance value for the AuNP decorated, WS_2 incorporated PEDOT-PSS electrode is 12.97 Ω. The R_{ct} value increases to 45.33 Ω after glutaraldehyde uptake as thin neutral layer of glutaraldehyde over the polymer composite surface obstruct the flow of electrons at the interface. Further, increase in R_{ct} value after antibody treatment up to 127.8 Ω suggests effective binding of the anti-AF-B_1 over the surface of the electrode. Upon interaction with the analyte (AF-B_1), the R_{ct} value again increases to 374.2 Ω owing to the formation of dielectric layer at the electrode – electrolyte interface.

There is also an increase in Q_2 value after glutaraldehyde treatment. This may be due to the presence of reactive di-aldehydic groups on the electrode surface, thus resulting in an increase in electroactive areas at the interface. Slight increase in the value after antibody treatment results in the effective attachment of the biomolecules over the electrode surface. A significant increase in Q_2 after binding to antigen is observed, probably due to the closely bound antibody-antigen complex related to conformational changes within the proteins structure. Changes in the Q_3 value after every step leads to space charge layer modification between the PEDOT and PSS rich grains in presence of WS_2 and AuNPs in between. An increase in W_3 values after each step indicates a significant increase in diffusional impedance mainly because of the conformational changes within antibody - antigen proteins, which were associated with the introduction of porous layers after each step.

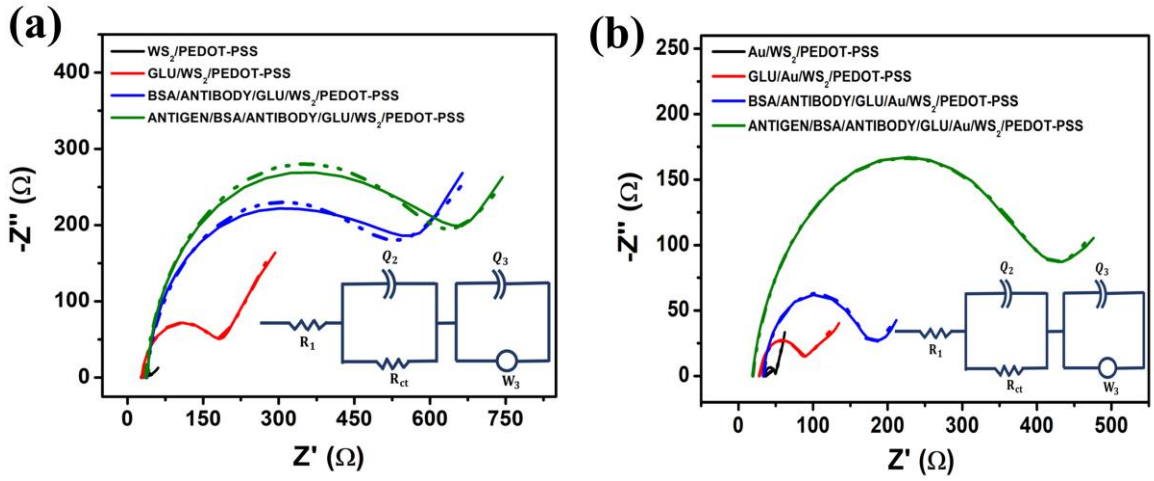

Figure 5.9: Impedance plot of (a) WS_2/PEDOT-PSS and (b) AuNP/WS_2/PEDOT-PSS films on ITO electrode after each process. The inset shows the equivalent circuit.

Table 5.3: Fitted parameters of impedance spectra for AuNP/WS_2/PEDOT-PSS/ITO electrode after every process step and after addition of AF-B_1.

Serial number	Electrode	R_1 (Ω)	R_{ct} (Ω)	Q_2 ($\times 10^{-6}$) $S.s^n$	Q_3 ($\times 10^{-3}$) $S.s^n$	W_3 ($x10^{-6}$) ($S.s^{1/2}$)
1	AuNP/WS_2/PEDOT-PSS	36.31	12.97	6.732 $n = 0.980$ $Q_2{}^n = 6.45$	6.824 $n = 0.756$ $Q_2{}^n = 4.27$	55.03
2	GLU/AuNP/WS_2/ PEDOT-PSS	27.92	45.33	7.789, $n = 1$ $Q_2{}^n = 7.78$	5.447, $n = 0.4$ $Q_3{}^n = 1.96$	746
3	Antibody/BSA/GLU/ AuNP/WS_2/PEDOT-PSS	33.30	127.8	12.05, $n = 0.944$ $Q_2{}^n = 10.48$	4.760, $n = 0.5$ $Q_3{}^n = 2.18$	1853
4	ANTIGEN/Antibody/ BSA/GLU/AuNP/ WS_2/PEDOT-PSS	19.27	374.2	18.75, n = 0.884 $Q_2{}^n = 13.34$	0.232, n = 0.895 $Q_3{}^n = 0.27$	2735

5.8. Transient capacitance measurement of AF-B_1 sensor and selectivity

In a label-free immunosensor that does not utilize enzymes or redox agents, it is possible to determine the maximum change that results from antibody and antigen interactions due to formation of additional dielectric layer at the surface of the electrode by measuring the transient capacitance at a medium or low frequency [26]. Because electrodes and electrolytes interact to form an electrolytic capacitor, the detection of the analyte is therefore carried out by transient capacitance measurement (parallel capacitance versus time) at a fixed bias voltage of 0.8 volts. For single frequency transient capacitance measurement, two frequencies are chosen: 77 Hz (a lower frequency) and 1 kHz (a medium frequency). The transient capacitance plots at 77 Hz and 1 kHz are shown in Figure 5.10 (a) and (b); respectively. As can be found in respective plots after obtaining a stable baseline, different concentrations of antigen AF- B_1 were injected into the electrolyte PBS. The baseline shows systematic decrease in the capacitance response at each subsequent addition of antigen AF- B_1 because of formation of dielectric layer at the interface owing to antigen – antibody binding. Furthermore, the selectivity of the sensor was examined by using human serum IgG, a non-specific protein molecule for the immobilized anti - AF-B_1. Upon addition of human serum IgG the capacitive response increases but drops quickly

to retain the earlier trend at 77 Hz. Again at 1 kHz, the sensor did not show any observable change while human serum IgG was added, indicating no interaction with anti- AF-B_1. Therefore, the proposed immunosensor is highly selective towards AF- B_1 only, as confirmed both at 77 Hz and 1 kHz.

Afterwards, the change in capacitive response (ΔC_p) at each subsequent antigenic addition versus concentration (at both the frequency: 77 Hz and 1 kHz) for the Au decorated WS_2 incorporated PEDOT-PSS based ITO electrode has been plotted, depicted in Figure 5.10 (c). The sensor shows two linear trends within two different concentrations for both the frequencies.

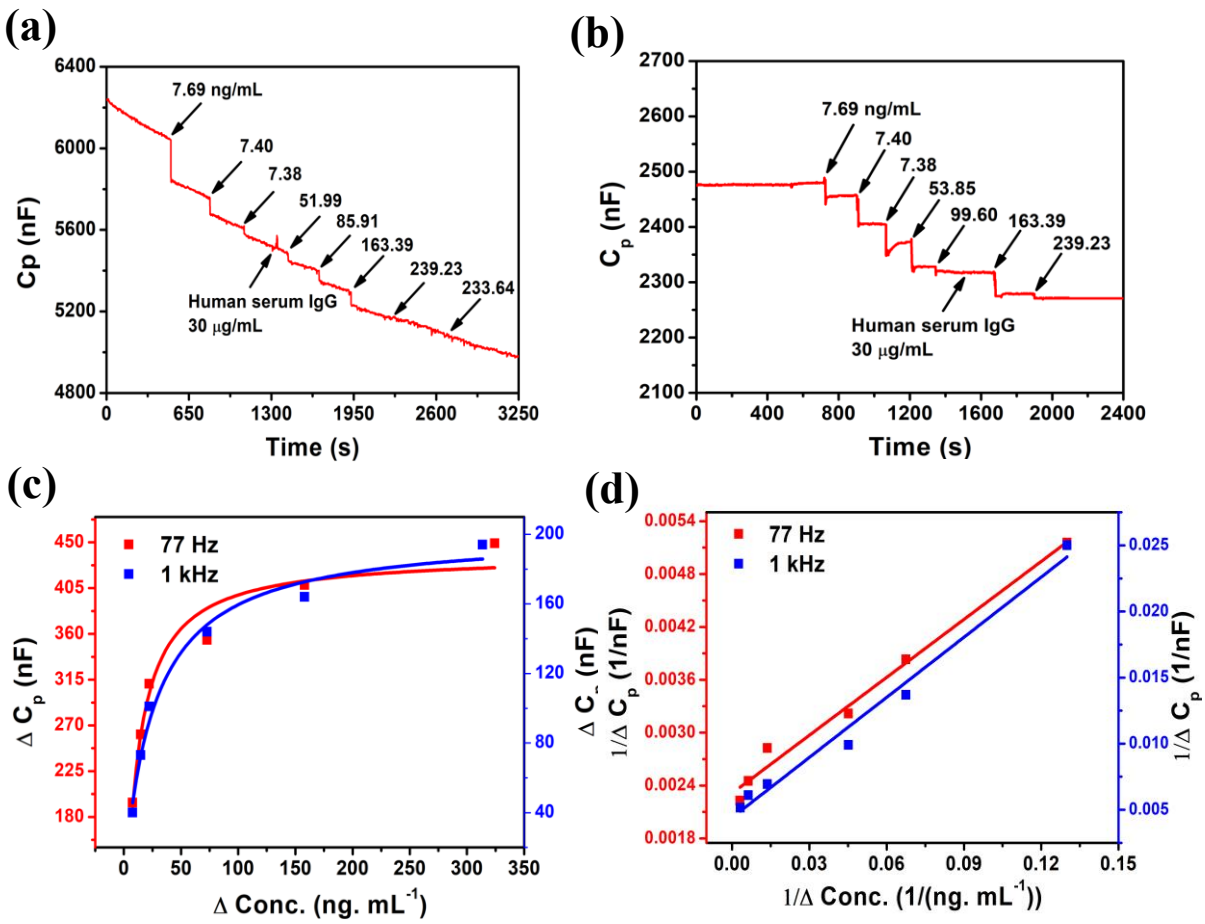

Figure 5.10: Transient capacitance plot of anti-AF-B_1/GLU/Au/WS_2/PEDOT-PSS based AF-B_1 sensors at (a) 77 Hz (b) 1 kHz; at a DC bias voltage of 0.8 V. (c) Adsorption plot and (d) Linear regression plot of Au/WS_2/PEDOT-PSS capacitive sensor at 77 Hz and 1 kHz.

At 77 Hz, there is a smooth augment in the sensor response from 7.69 ng mL^{-1} to 59.41 ng mL^{-1}, following that there is a steady response beyond this concentration from 59.41 ng mL^{-1} to 324.32 ng mL^{-1} and further leads to saturation. Similarly at 1 kHz, the sensor response increases rapidly within the concentration range from 7.69 ng mL^{-1} to 68.08 ng mL^{-1} with a subsequent steady response from 68.08 ng mL^{-1} to 313.72 ng mL^{-1} and rises to saturation.

Using the adsorption isotherm equation, which is

$$C_p = \frac{A}{(1+\frac{B}{[C]})} \tag{5.2}$$

where C_p denotes change in the capacitance value, [C] represents change in the analyte concentration, with both A and B as constants. A being the saturated capacitance response and B is the inverse value of adsorption coefficient. Moreover, inverse of C_p versus inverse of antigen concentration is plotted for both 77 Hz and 1 kHz (Figure 5.10 (d)). From the linear regression plot, the LOD's are calculated for both the frequency and found to be 30.97 ng mL^{-1} (206 pM) at 77 Hz and 31.40 ng mL^{-1} (209 pM) at 1 kHz [21]. The sensor response is estimated to be 45.62 nF.ng^{-1} mL and 6.60 nF. ng^{-1} mL at 77 Hz and 1 kHz respectively.

5.9. Repeatability

Furthermore, for the development of a reliable biosensor, repeatability was carried out with different AuNPs anchored WS_2 incorporated PEDOT-PSS based electrodes at both frequencies (77 Hz and 1 kHz). The repeatability was evaluated by running the experiment with same optimized condition in presence of three different electrodes and the results endorsed good repeatability, as can be found in Table 5.4, having LOD value ~ 33 ng mL^{-1} and ~ 40 ng mL^{-1} at 77 Hz and 1 kHz; respectively. The linear plot of $1/\Delta C_p$ vs. $1/\Delta$Conc with error bars at both 77 Hz and 1 kHz is shown in Figure 5.11.

Table 5.4: Results from repeated experiments for AF-B_1 capacitive sensor (both at 77 Hz and 1 kHz).

Serial number	Electrode	Frequency, Hz	LOD, (ng mL^{-1})	Sensitivity, ($nFng^{-1}$ mL)	Linear range, (ng mL^{-1})
1	AuNP/WS_2/PEDOT-PSS, sensor 1	77	30.97	1/ 0.02192 = 45.62	7.69 - 324.32
2	AuNP/WS_2/PEDOT-PSS, sensor 2	77	33.33	1/ 0.01802 = 55.49	7.69 - 324.32
3	AuNP/WS_2/PEDOT-PSS, sensor 3	77	37.87	1/ 0.08784 = 11.38	7.69 - 324.32
4	AuNP/WS_2/PEDOT-PSS, sensor 1	1000	31.40	1/ 0.15158 = 6.59	7.69 - 324.32
5	AuNP/WS_2/PEDOT-PSS, sensor 2	1000	44.36	1/0.12469 = 8.01	7.69 - 324.32
6	AuNP/WS_2/PEDOT-PSS, sensor 3	1000	46.15	1/ 0.09069 = 11.02	7.69 - 324.32

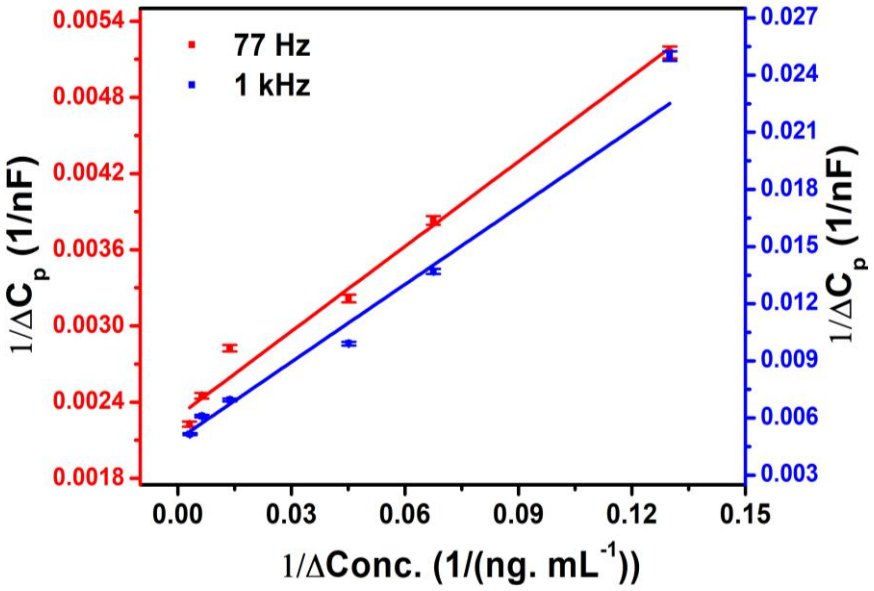

Figure 5.11: Linear regression plot of AuNP/WS_2/PEDOT-PSS capacitive sensors at 77 Hz and 1 kHz; with error bar.

5.10. Differential Pulse Voltammetry response of AF-B_1 sensor

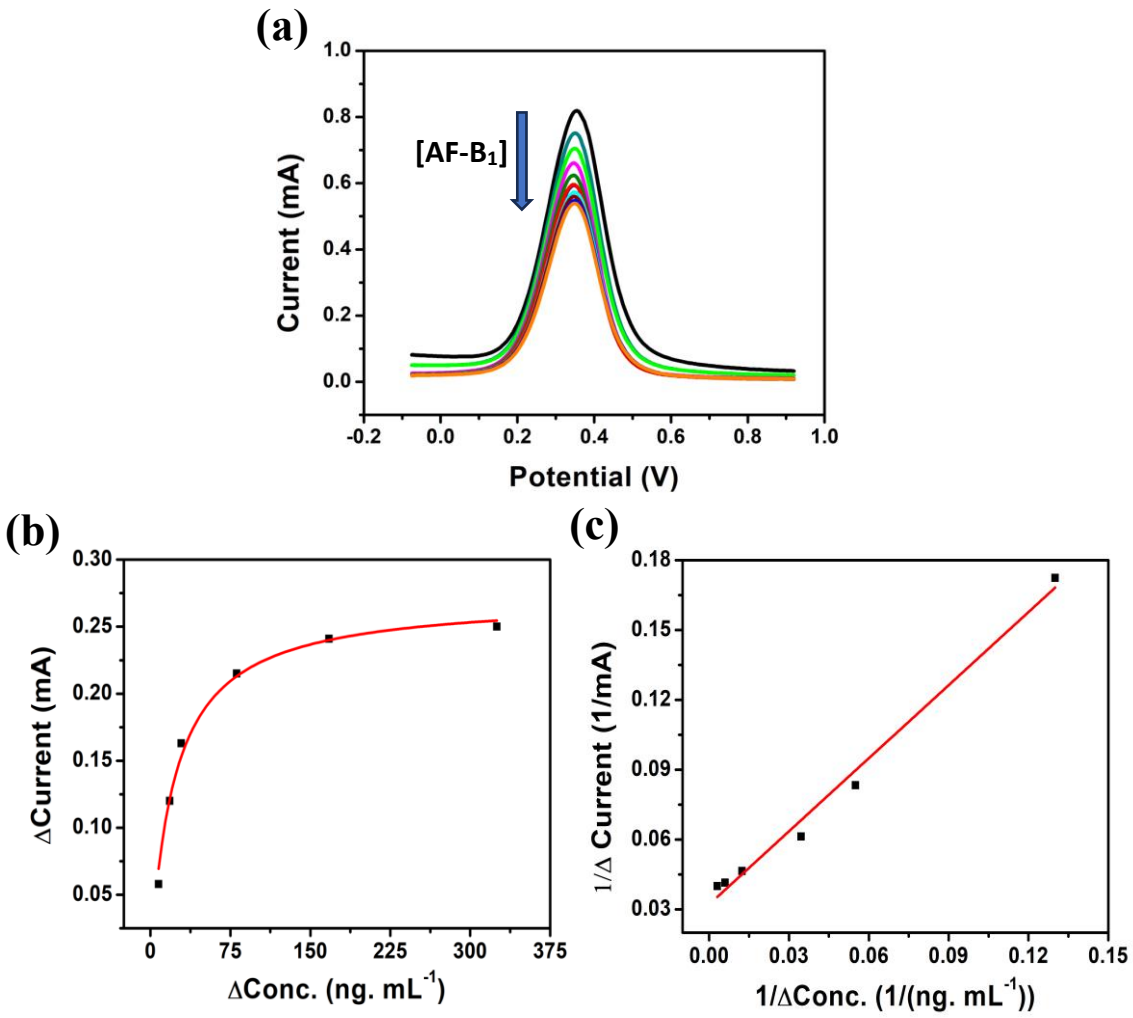

Figure 5.12: DPV plot of BSA/anti-AF-B_1/GLU/AuNPs/WS_2/PEDOT-PSS/ITO with different concentration of AF-B_1 (7.69 ng mL^{-1}-654.25 ng mL^{-1}) (b) Adsorption isotherm plot. (c) Linear regression plot for 1/ΔConc. vs. 1/ΔCurrent.

To study the performance of the immunosensor towards detection of AF-B_1, another technique, DPV was carried out on anti-AF-B_1 immobilized immunosensor. A sophisticated electrochemical technique can be utilized to study the electrochemical amperometric responses. The DPV responses of the AuNPs anchored WS_2 incorporated PEDOT-PSS based electrodes modified with antibody anti-AF-B_1 towards different concentrations of AF-B_1 are depicted in Figure 5.12 (a). The DPV was performed by taking the potential from -0.2 V to 0.8 V in a three - electrode setup in presence of 500 mM $[Fe(CN)_6]^{3-/4-}$ + 100 mM PBS as an electrolyte. The DPV plot shows systematic decrement

in the current response with added concentration of analyte AF-B_1 indicating specific interaction between anti-AF-B_1 and AF-B_1. Apparently, the formation of antibody and antigen complexes on the bioelectrode prevents electron transfer between the redox probe $[Fe(CN)_6]^{3-/4-}$ and the electrode.

Afterwards, a change in the DPV peak current for BSA/anti-AF-B_1/GLU/Au/WS_2/PEDOT-PSS/ITO electrode versus change in AF-B_1 concentration was plotted, shown in Figure 5.12 (b). Next, Δ Current versus Δ Concentration was fitted using Langmuir adsorption isotherm (equation 4.3, chapter 4). In this case, *x* represents change in antigenic concentration and *Y* denotes the response of change in current. Here, *A* and *B* both are constants, *A* is the saturated current response while *B* is the inverse of adsorption coefficient. As can be seen from Figure 5.12 (b), the sensor characterized a linear rapid response at the lower concentration from 7.69 ng mL^{-1} to 92.88 ng mL^{-1} and subsequently a steady state within the concentration range from 92.88 ng mL^{-1} to 325.04 ng mL^{-1} and eventually saturated with no increase in the current response. A linear regression plot between inverse of Δ Current and inverse of Δ Conc. is shown in Figure 5.12 (c) having correlation coefficient, R^2 value 0.9879. The detection limit is found to be 37.87 ng mL^{-1} (252 pM). The sensitivity of the proposed sensor is estimated to be 9.55 $\mu Ang^{-1}mL$.

5.11. Repeatability and selectivity

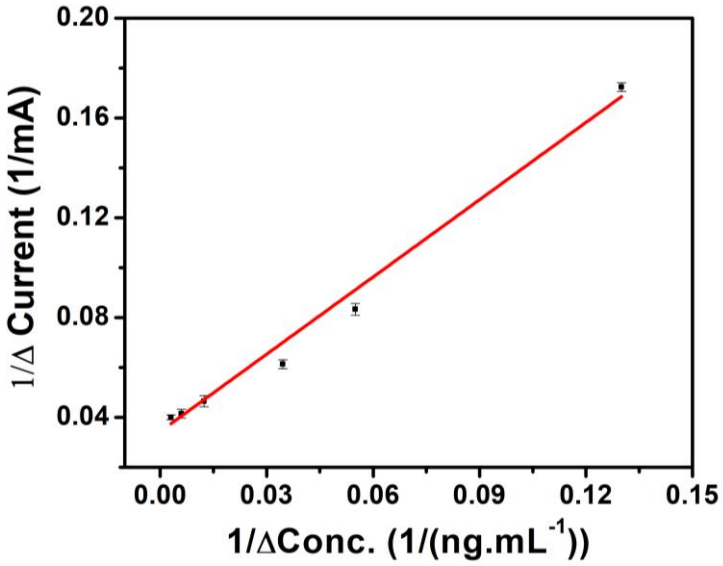

Figure 5.13: 1/ΔI vs. 1/ΔConc. for the BSA/anit-AF-B_1/GLU/AuNP/WS_2/PEDOT-PSS sensor along with linear regression plot with error bar w.r.to standard deviation.

Interestingly, comparable results could be traced from repeatable experiments with different electrodes, as displayed in Table 5.5. The linear plot obtained with the error bars for BSA/anti-AF-B_1/GLU/Au/WS_2/PEDOT-PSS/ITO electrode can be found in Figure 5.13. Data displays very good repeatability with LOD value, 37-43 ng mL^{-1} (238-277 pM). Both capacitive and DPV methods showed comparable results.

Table 5.5: Results of repeated experiments for Au/WS_2/PEDOT-PSS based AF-B_1 sensor using amperometry technique, (DPV).

Serial number	Electrode	LOD, (ng mL^{-1})	Sensitivity, ($\mu Ang^{-1}mL$)	Linear range, (ng mL^{-1})
1	AuNP/WS_2/PEDOT-PSS, sensor 1	37.87	1/ 104.67 = 9.55	7.69 – 325.04
2	AuNP/WS_2/PEDOT-PSS, sensor 2	37.34	1/ 105.22 = 9.50	7.69 – 325.04
3	AuNP/WS_2/PEDOT-PSS, sensor 3	42.45	1/ 104.92 = 9.53	7.69 – 325.04

The selectivity of the sensor was evaluated using human serum IgG non- specific protein molecules. Upon injection of human serum IgG, the sensor did not show any change or shift in the DPV peak current, as evident from the response shown in Figure 5.14. Thus, the proposed sensor is highly selective towards its specific analyte only i.e. AF-B_1.

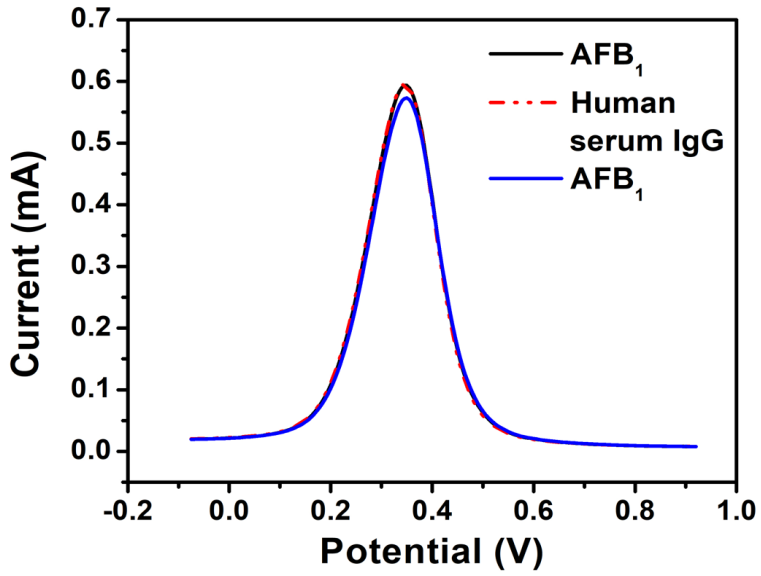

Figure 5.14: Selectivity test of BSA/anit-AF-B_1/GLU/AuNP/WS_2/PEDOT-PSS sensor.

5.12. Real sample analysis

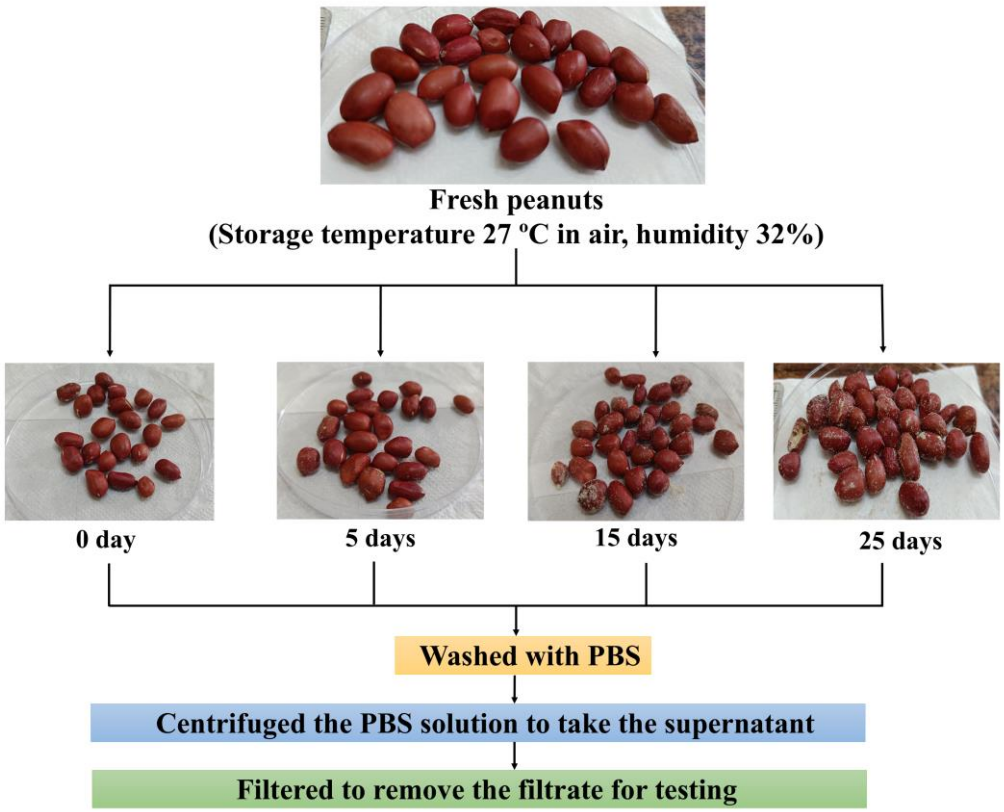

Figure 5.15: Scheme for testing peanuts of different days of air exposure at a temperature of 27 ºC after obtaining from local source.

In order to implement the proof of concept for real samples, DPV was performed on BSA/anti-AF-B_1/GLU/AuNP/WS_2/PEDOT-PSS/ITO immunosensor with real sample peanuts, scientific name: *Arachis hypogaea*, purchased from market. The preparation steps of peanuts sample for testing are represented via a schematic, shown in Figure 5.15. In this evaluation, peanuts were stored at a temperature of ~27 ºC in air (humidity~32%) for five, fifteen and twenty-five days. The DPV measurements were taken using PBS to wash both fresh peanuts and stored peanuts with repeated spiking ranging from 50 to 300 µL. The DPV current response of different days of air exposure peanuts with repeated spiking of (50-300 µL) is shown in Figure 5.16 (a-d) respectively. Additionally, the variation in DPV peak current for each spike, as a function of the number of days, is presented in Figure 5.17. This indicates the presence of 24.01 ng mL^{-1} of AF-B_1 in the peanuts after twenty-five days of exposure at room temperature.

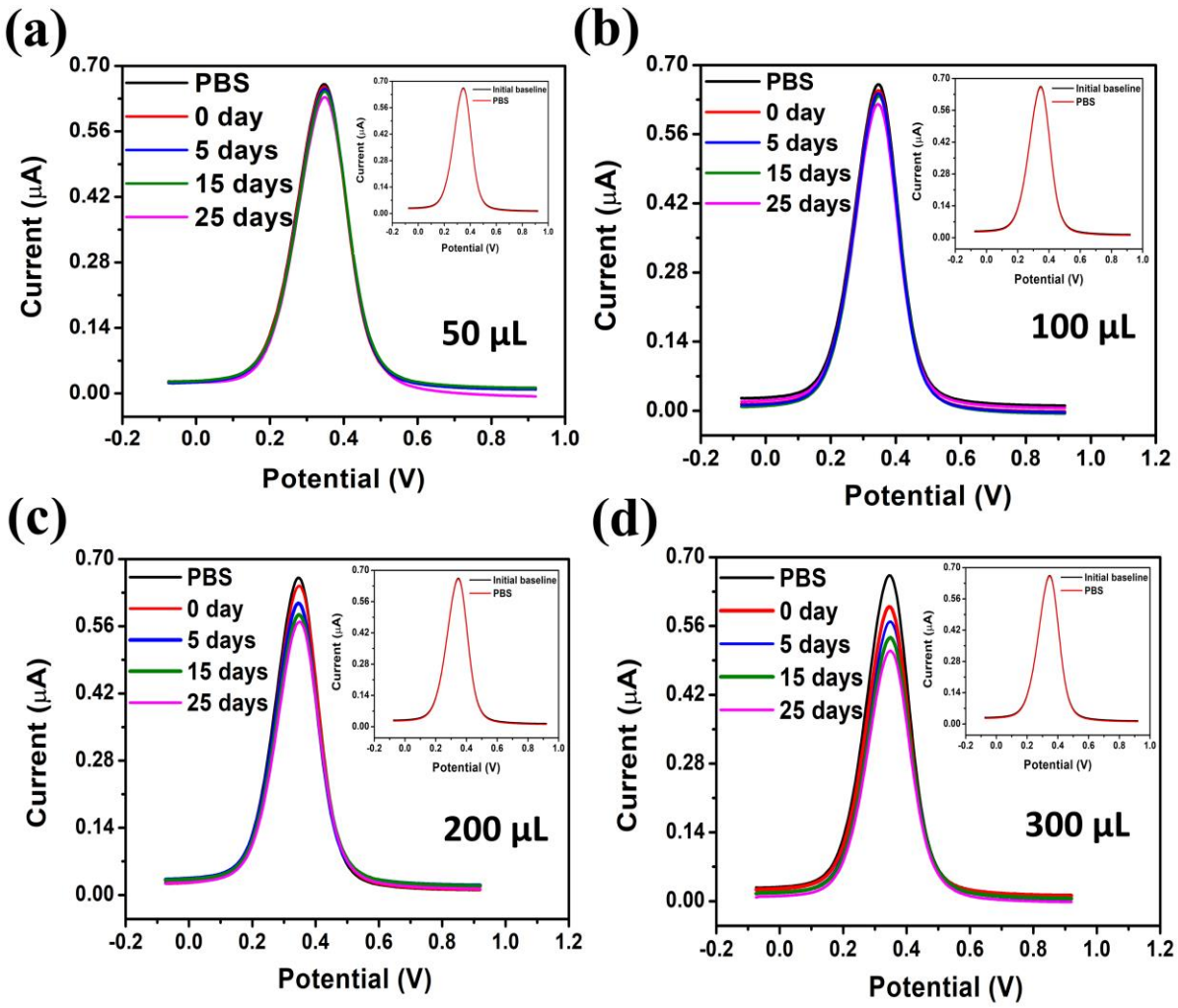

Figure 5.16: DPV pattern of AuNP/WS_2/PEDOT-PSS/ITO composite electrode towards peanuts (kept exposed to air 27 ºC for 0-25 days and washed with PBS) with different spiking volumes (50-200) µL, (a) 50 µL (b) 100 µL, (c) 200 µL (d) 300 µL. Inset shows the voltammogram after addition of 200 µL PBS.

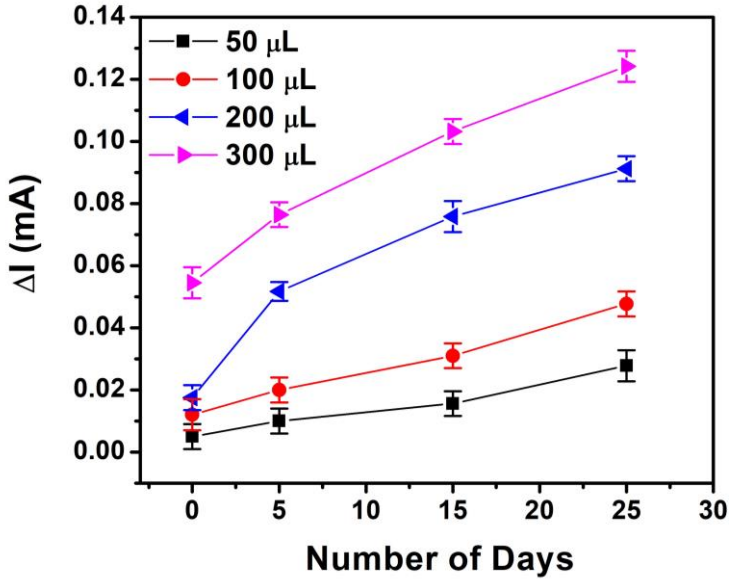

Figure 5.17. Change in peak current vs number of days of air exposure for peanuts.

5.13. Conclusions

AuNP decorated WS_2 anchored PEDOT-PSS based ITO electrode was studied for highly sensitive, selective and reliable glucose sensing and AF-B_1 sensing. Glucose sensing was carried out with *GlOx*/GLU/AuNP/WS_2/PEDOT-PSS/ITO and AF-B_1 sensing was performed using anti-AF-B_1/GLU/AuNP/WS_2/PEDOT-PSS/ITO electrodes respectively. From electrochemical investigation of the electrodes, it has been found that, with Au nanoparticle incorporation over WS_2 modified PEDOT-PSS/ITO electrode, the conductivity and catalytic activity increased and the films became more stable. Further for biosensor fabrication, the functionalization of the modified electrodes was done by using glutaraldehyde cross linker. From the systematic cyclic voltammetric study, direct electron transfer to the Au nanoparticle incorporated composite electrodes was observed after the glucose interaction with immobilized *GlOx* enzyme. The entrapped *GlOx* enzyme exhibited good linearity towards oxidation of glucose on fabricated AuNP/WS_2/PEDOT-PSS/ITO electrode. Glucose sensor based on AuNP/WS_2/PEDOT-PSS/ITO electrode depicted fast and consistent response with better linearity within the range of 0.74 to 440.67 µM, LOD 1 µM and sensitivity of 13.1 µA μM^{-1}. When compared to our previous system (AuNP/GO/PEDOT-PSS/ITO), the AuNP/WS_2/PEDOT-PSS/ITO electrode exhibited better performance towards oxidation of glucose. Further, the sensors were found to be highly selective towards glucose. The developed biosensors were finally tested for

human saliva samples yielding encouraging performance with excellent repeatability. As for AF-B_1 detection, a label free immunosensor was fabricated by immobilizing anti-AF-B_1 onto the system in presence of glutaraldehyde cross linking agent. Electrochemical characterization, cyclic voltammetry and electrochemical impedance spectroscopy of the AuNP/WS_2/PEDOT-PSS system resulted in excellent electroactive properties and charge transfer kinetics. Sensor fabrication process steps were also studied through CV and EIS. Two sensing techniques namely transient capacitance and DPV were employed and compared the results. From Transient capacitance measurements, the BSA/Anti-AF-B_1/GLU/AuNP/WS_2/PEDOT-PSS/ITO sensor yielded a response of 45.62 $nFng^{-1}mL$ and 6.60 $nFng^{-1}mL$ at 77 Hz and 1 kHz respectively. The respective LOD's were found to be 30.97 ng mL^{-1} (206 pM) and 31.40 ng mL^{-1} (209 pM). The linear range of the proposed sensor was estimated to be within the concentration range from 7.69 ng mL^{-1} to 324.32 ng mL^{-1} at 77 Hz and 7.69 ng mL^{-1} - 313.72 ng mL^{-1} at 1 kHz. The amperometry sensing performance with anti-AF-B_1 immobilized BSA/Antibody/GLU/AuNP/WS_2/PEDOT-PSS/ITO sensor showed a wide linear range within 7.69 ng mL^{-1} - 325.04 ng mL^{-1} and with a response of 9.55 $\mu Ang^{-1}mL$. The corresponding LOD from the DPV experiment was calculated to be 37.87 ng mL^{-1}. The selectivity of the sensor was examined with both the sensing technique using non - specific protein molecule human serum IgG and the sensor was found to be highly selective towards AF-B_1 only. The sensing parameters evaluated from both the capacitive and amperometric methods are quite comparable. Real sample analysis with the proposed immunosensor with peanuts provide the best feasible solution for onsite detection of AF-B_1. In case of 2D WS_2, easy exfoliation from bulk to a few layers could be facilitating the interlayer separation overcoming the weak Van der Waals forces, resulting in increased surface area in the AuNP/WS_2/PEDOT-PSS/ITO electrode leading to wider sensing range and higher sensitivity compared to GO based composites, AuNP/GO/PEDOT-PSS. The use of different nanostructure, especially one-dimensional nanofibers to further enhance the analytical parameters of glucose sensor and AF-B_1 sensor shall be discussed in subsequent chapter.

5.14. References

[1] Wang, L., Xu, D., Jiang, L., Gao, J., Tang, Z., Xu, Y., ... and Zhang, H. Transition metal dichalcogenides for sensing and oncotherapy: status, challenges, and perspective. *Advanced Functional Materials*, 31(5):2004408, 2021.

[2] Rohaizad, N., Mayorga-Martinez, C. C., Sofer, Z., and Pumera, M. 1T-phase transition metal dichalcogenides (MoS2, MoSe2, WS2, and WSe2) with fast heterogeneous electron transfer: application on second-generation enzyme-based biosensor. *ACS applied materials & interfaces*, 9(46):40697-40706, 2017.

[3] Li, Y., Fan, C., and Zheng, J. A high-efficiency electrochemical sensor of dopamine based on WS2 nanosheets decorated with dandelion-like platinum–silver nanoparticles. *Journal of Materials Science: Materials in Electronics*, 33(8):5061-5072, 2022.

[4] Meng, S., Zhang, Y., Wang, H., Wang, L., Kong, T., Zhang, H., and Meng, S. Recent advances on TMDCs for medical diagnosis. *Biomaterials*, 269:120471, 2021.

[5] Bahri, M., Yu, D., Zhang, C. Y., Chen, Z., Yang, C., Douadji, L., and Qin, P. Unleashing the potential of tungsten disulfide: Current trends in biosensing and nanomedicine applications. *Heliyon*. 10(2):e24427, 2024.

[6] Hao, J., Song, G., Liu, T., Yi, X., Yang, K., Cheng, L., and Liu, Z. In vivo long-term biodistribution, excretion, and toxicology of PEGylated transition-metal dichalcogenides MS2 (M= Mo, W, Ti) nanosheets. *Advanced Science*, 4(1):1600160, 2017.

[7] Teo, W. Z., Chng, E. L. K., Sofer, Z., and Pumera, M. Cytotoxicity of exfoliated transition-metal dichalcogenides (MoS2, WS2, and WSe2) is lower than that of graphene and its analogues. *Chemistry–A European Journal*, 20(31):9627-9632, 2014.

[8] Rohaizad, N., Mayorga-Martinez, C. C., Sofer, Z., and Pumera, M. 1T-phase transition metal dichalcogenides (MoS2, MoSe2, WS2, and WSe2) with fast heterogeneous electron transfer: application on second-generation enzyme-

based biosensor. *ACS applied materials & interfaces*, 9(46):40697-40706, 2017.

[9] Wang, T., Liu, C., Wang, X., Li, X., Jiang, F., Li, C., ... and Xu, J. Highly enhanced thermoelectric performance of WS2 nanosheets upon embedding PEDOT: PSS. *Journal of Polymer Science Part B: Polymer Physics*, 55(13):997-1004, 2017.

[10] Baharin, S. N. A., Samsudin, N. S., Suhaimi, N. F., and Sambasevam, K. P. Potential applications of Conducting Polymer/Tungsten Disulfide Composites: A Mini Review. *Malaysian Journal of Analytical Sciences*, 26(2):251-268, 2022.

[11] Villamayor, M. M. S., Lindblad, A., Johansson, F. O., Tran, T., Pham, N. H., Primetzhofer, D., ... and Nyberg, T. Growth of two-dimensional WS2 thin films by reactive sputtering. *Vacuum*, 188:110205, 2021.

[12] Sarfraz, N., and Khan, I. Plasmonic gold nanoparticles (AuNPs): properties, synthesis and their advanced energy, environmental and biomedical applications. *Chemistry–An Asian Journal*, 16(7):720-742, 2021.

[13] Ramalingam, V. Multifunctionality of gold nanoparticles: Plausible and convincing properties. *Advances in colloid and interface science*, *271*:101989, 2019.

[14] Falahati, M., Attar, F., Sharifi, M., Saboury, A. A., Salihi, A., Aziz, F. M., ... and El-Sayed, M. A. Gold nanomaterials as key suppliers in biological and chemical sensing, catalysis, and medicine. *Biochimica et Biophysica Acta (BBA)-General Subjects*, 1864(1):129435, 2020.

[15] Mazeiko, V., Kausaite-Minkstimiene, A., Ramanaviciene, A., Balevicius, Z., and Ramanavicius, A. Gold nanoparticle and conducting polymer-polyaniline-based nanocomposites for glucose biosensor design. *Sensors and Actuators B: Chemical*, 189:187-193, 2013.

[16] Zhang, B. L., Yang, Y., Zhao, Z. Q., and Guo, X. D. A gold nanoparticles deposited polymer microneedle enzymatic biosensor for glucose sensing. *Electrochimica Acta*, 358:136917, 2020.

[17] Chi, Q., Zhang, J., Dong, S., and Wang, E. Direct electrochemistry and surface characterization of glucose oxidase adsorbed on anodized carbon electrodes. *Electrochimica Acta*, *39*(16):2431-2438, 1994.

[18] Zhang, X., Liu, D., Li, L., and You, T. Direct electrochemistry of glucose oxidase on novel free-standing nitrogen-doped carbon nanospheres@ carbon nanofibers composite film. *Scientific reports*, 5(1):9885, 2015.

[19] Muguruma, H., Iwasa, H., Hidaka, H., Hiratsuka, A., and Uzawa, H. Mediatorless direct electron transfer between flavin adenine dinucleotide-dependent glucose dehydrogenase and single-walled carbon nanotubes. *ACS Catalysis*, 7(1):725-734, 2017.

[20] Lipinska, W., Siuzdak, K., Karczewski, J., Dołęga, A., and Grochowska, K. Electrochemical glucose sensor based on the glucose oxidase entrapped in chitosan immobilized onto laser-processed Au-Ti electrode. *Sensors and Actuators B: Chemical*, *330*, 129409, 2021.

[21] Shrivastava, A., and Gupta, V. B. Methods for the determination of limit of detection and limit of quantitation of the analytical methods. *Chronicles of Young Scientists*, 2(1):21-25, 2011.

[22] Kadian, S., Arya, B. D., Kumar, S., Sharma, S. N., Chauhan, R. P., Srivastava, A., ... and Singh, S. P. Synthesis and application of PHT-TiO_2 nanohybrid for amperometric glucose detection in human saliva sample. *Electroanalysis*, 30(11):2793-2802, 2018.

[23] Gligor, D., Cuibus, F., Peipmann, R., and Bund, A. Novel amperometric sensors for nitrite detection using electrodes modified with PEDOT prepared in ionic liquids. *Journal of Solid State Electrochemistry*, 21:281-290, 2017.

[24] Sharma, A., Kumar, A., and Khan, R. A highly sensitive amperometric immunosensor probe based on gold nanoparticle functionalized poly (3, 4-ethylenedioxythiophene) doped with graphene oxide for efficient detection of aflatoxin B1. *Synthetic Metals*, *235*:136-144, 2018.

[25] Baruah, B., Kumar, A., Umapathy, G. R., and Ojha, S. Enhanced electrocatalytic activity of ion implanted rGO/PEDOT:PSS hybrid nanocomposites towards methanol electro-oxidation in direct methanol fuel cells. *Journal of Electroanalytical Chemistry*, 840:35-51, 2019.

[26] Baruah, S., Mohanta, D., and Betty, C. A. Highly sensitive and label free on-site monitoring immunosensor for detection of Aflatoxin B_1 from real samples. *Analytical Biochemistry*, 689:115493, 2024.